Selective Laser Melting processed Ti6Al4V lattices with graded porosities for dental applications

WALLY, Z, HAQUE, A, FETEIRA, Antonio <http://orcid.org/0000-0001-8151-7009>, CLAEYSSENS, F, GOODALL, R and REILLY, G

Selective Laser Melting processed Ti6Al4V lattices with graded porosities for dental applications

Zena J Wally, Abdul M Haque, Antonio Feteira, Frederik Claeyssens, Russell Goodall, Gwendolen C Reilly

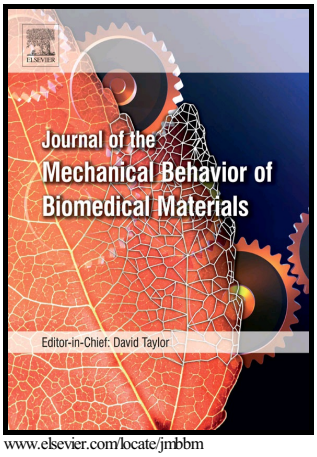

www.elsevier.com/locate/jmbbm

PII: S1751-6161(18)30619-2
DOI: https://doi.org/10.1016/j.jmbbm.2018.08.047
Reference: JMBBM2958

To appear in: *Journal of the Mechanical Behavior of Biomedical Materials*

Received date: 25 January 2018
Revised date: 9 August 2018
Accepted date: 28 August 2018

Cite this article as: Zena J Wally, Abdul M Haque, Antonio Feteira, Frederik Claeyssens, Russell Goodall and Gwendolen C Reilly, Selective Laser Melting processed Ti6Al4V lattices with graded porosities for dental applications, *Journal of the Mechanical Behavior of Biomedical Materials,* https://doi.org/10.1016/j.jmbbm.2018.08.047

Selective Laser Melting processed Ti6Al4V lattices with graded porosities for dental applications

Zena J Wally [1, 2, 3, 4], Abdul M Haque [5], Antonio Feteira [6], Frederik Claeyssens [1, 2, 3], Russell Goodall [1] and Gwendolen C Reilly [1, 3]

[1] Department of Materials Science and Engineering, University of Sheffield, Sir Robert Hadfield Building, Mappin St, Sheffield S1 3JD, UK
[2] Kroto Research Institute, University of Sheffield, Broad Lane, Sheffield S3 7HQ, UK
[3] Insigneo Institute for in silico Medicine, University of Sheffield, Pam Liversidge Building, Mappin St, Sheffield S1 3JD, UK
[4] Department of Prosthodontic, College of Dentistry, University of Kufa, Najaf, Iraq.
[5] Medical Advanced Manufacturing Research Centre (AMRC), Wallis Way, Catcliffe, Rotherham, S60 5TZ, UK
[6] Materials Engineering and Research Institute, Sheffield Hallam University, Sheffield, S1 1WB, UK

E-Mail: g.reilly@sheffield.ac.uk

Abstract

Dental implants need to support good osseointegration into the surrounding bone for full functionality. Interconnected porous structures have a lower stiffness and larger surface area compared with bulk structures, and therefore are likely to enable better bone-implant fixation. In addition, grading of the porosity may enable large pores for ingrowth on the periphery of an implant and a denser core to maintain mechanical properties. However, given the small diameter of dental implants it is very challenging to achieve gradations in porosity. This paper investigates the use of Selective Laser Melting (SLM) to produce a range of titanium structures with regular and graded porosity using various CAD models. This includes a novel 'Spider Web' design and lattices built on a diamond unit cell. Well-formed interconnecting porous structures were successfully developed in a one-step process. Mechanical testing indicated that the compression stiffness of the samples was within the range for cancellous bone tissue. Characterization by scanning electron microscopy (SEM) and X-ray micro-computed tomography (μCT) indicated the designed porosities were well-replicated. The structures supported bone cell growth and deposition of bone extracellular matrix.

Graphical abstract:

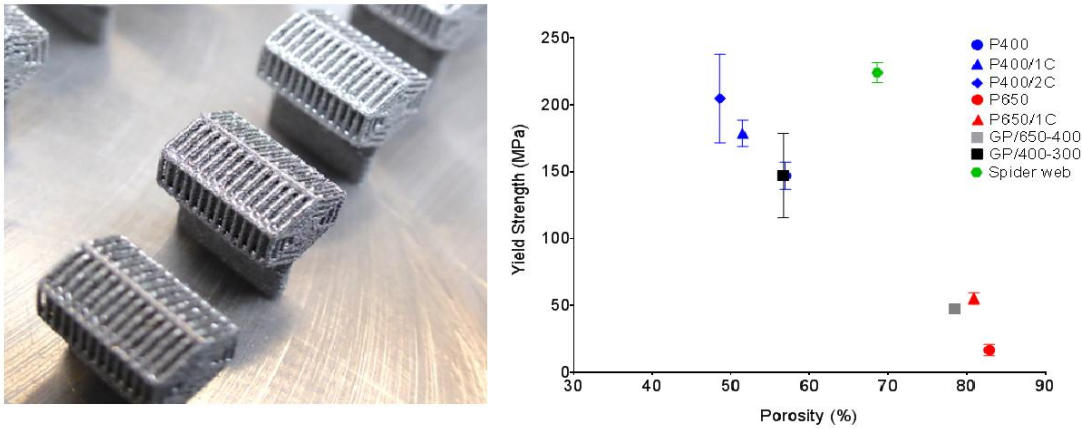

Keywords: porous titanium, dental implant, graded porosity, selective laser melting, bone growth, osteoblasts

1. Introduction

Oral implants have frequently been used to replace the root portions of natural teeth that have been lost due to fracture, periodontitis [1] or aging [2], to support the fixation of artificial teeth [3] and improve the function of mastication [4]. Following implant insertion into the jaw bone, three to six months of healing are required for the placement of fixed dental prostheses (crowns or bridges) and to obtain mineralized bone [5]. Although effective, up to 10 percent of dental implants fail to integrate with the bone as a result of poor bone quality and quantity [6]. Implant loosening is also reported in patients with poor bone healing, including smokers, diabetics [7], elderly people and those with osteoporosis [8]. There is therefore still the need for implants with improved ability to support ossoeintegration.

Titanium and Ti-6Al-4V have been employed for dental and orthopaedic applications due to their excellent properties such as good biocompatibility, high corrosion resistance and high strength to weight ratio [9]. Bulk 'titanium-based' devices have been the traditional form used for dental implants, but the Young's modulus of solid titanium is much higher than that of bone [2]. This may cause the load distribution between hard tissue and the implant to be non-uniform, and researchers have suggested that this leads to 'stress shielding' and bone resorption, resulting in the loosening and failure of the implant [1]. Porous titanium structures have the advantage that their effective stiffness can be manipulated to match bone tissue [10] and that the porosity provides a larger surface area, which in turn encourages the attachment and proliferation of bone cells, enables bone ingrowth into the material and improves osseointegration [11]. A high surface area eliminates early micromotion of implants [12] which promotes fibrous tissue rather than osseointegration and cause initial instability [13]. Since pore parameters such as size, shape and the overall amount of porosity have been shown to play a vital role in bone cell ingrowth [14], this necessitates using a processing method able to produce optimal porosity in a metallic biomaterial, as achieving both the required biological and mechanical properties is essential for implant applications.

Several studies have successfully created titanium foams or lattices either for coating or within the bulk of a structure for varied applications using processing methods such as metal injection moulding of Ti foam [15]. In recent years, additive manufacturing, including Electron Beam Melting (EBM) and Selective Laser Melting (SLM) have been increasingly considered as economically viable techniques to fabricate challenging structures [16]. With SLM, dental and orthopaedic implant prototypes have been developed with complex pore geometries by melting Ti powder microparticles using a focused laser beam according to a computer-generated three-dimensional design [17, 18, 19]. An inert gas or a vacuum is used during the fabrication process to manufacture titanium parts which are easily oxidised in air [16]. However porosity within the bulk metal structure (not indended as part of the overall design) reduces mechanical properties, and as a result, unless this can be controlled, such materials are unlikely to be used for bone replacement devices in load-bearing areas [20]. In an attempt to withstand physiological loads, a structure with a dense core and porous shell has been suggested, which might be more acceptable for oral implantology [21]. Another suggestion includes graded porous architecture with a stiff core, where the core will provide mechanical stability and the graded porosity allows ingrowth [22]. Such a structure could also reduce the stress concentrations occurring on loading between adjacent layers with very different Young's moduli [23], as can happen when porous materials are bonded to dense materials.

With the breadth and versatility of processing methods, the optimal pore structure for bone cell ingrowth remains to be elucidated. Here we aim to compare a range of porous titanium lattices of approximately cylindrical form, which could form the basis of a porous dental implant. In this study, the Selective Laser Melting (SLM) process was used with Ti-6Al-V to build a range of titanium micro-lattice structures. Variable pore sizes and strut thicknesses were used to create regular and

graded porous structures using a 'Spider Web' design and lattices based on a diamond unit cell. These lattices were tested under compression to determine their stiffness and strength, and in cell culture to test their ability to support bone cell growth.

2. Materials and Methods

2.1. Selective Laser Melting for the production of porous Ti6Al4V structures

SLM was used to process different porous titanium structures, employing a Renishaw AM250 system and spherical Ti6Al4V powder microparticles (grade 23) with particle sizes ranging from 15 - 55 µm. The machine was equipped with 200 W laser and used with a 70 µm diameter laser beam and 30 µm layer thickness, 5000 mm/s laser scan speed and 0.075 mm hatch distance. The data from the CAD model (STL format) of the structure are passed into the processing system and virtually sliced in 30-micron layers with a defined laser path. Slices are fused layer-by-layer over a number of hours to form components of porous and dense metal parts. To reduce the risk of oxidation and contamination, the building procedure was carried out under inert Ar gas. Materialise 3-Matics version 9.1 software was used to create different CAD concepts (table 1): lattice-based constructs were built on a diamond unit cell, applied to form approximately cylindrical structures with 5 mm diameter (figure 1a and b). Variants included different pore sizes and strut thicknesses, and the inclusion of a dense core of different diameters. In the diamond-based lattices, graded porosity was created by combining two layers of different strut thickness surrounding a dense core, which resulted in changes to the open 'pore size', with sizes of 400 and 650 µm and 300 and 400 µm being used for the inner and outer layer respectively. A 'spider web' design with 250 µm radial spokes and circumferential connecting struts was used to form titanium hexagonal prisms (diameter: 4.33 mm and height: 6.76 mm) (figure 1c). Each sample was positioned onto the software platform 30° from the wiper blade position, which was performed to ensure minimal forces were induced by contact with parts during powder re-coating. All sample components were loaded onto the build platform (Ti6Al4V) and positioned randomly. Lattice-based samples were built vertically on the build substrate while the 'Spider Web' samples were oriented horizontally (figure 2).

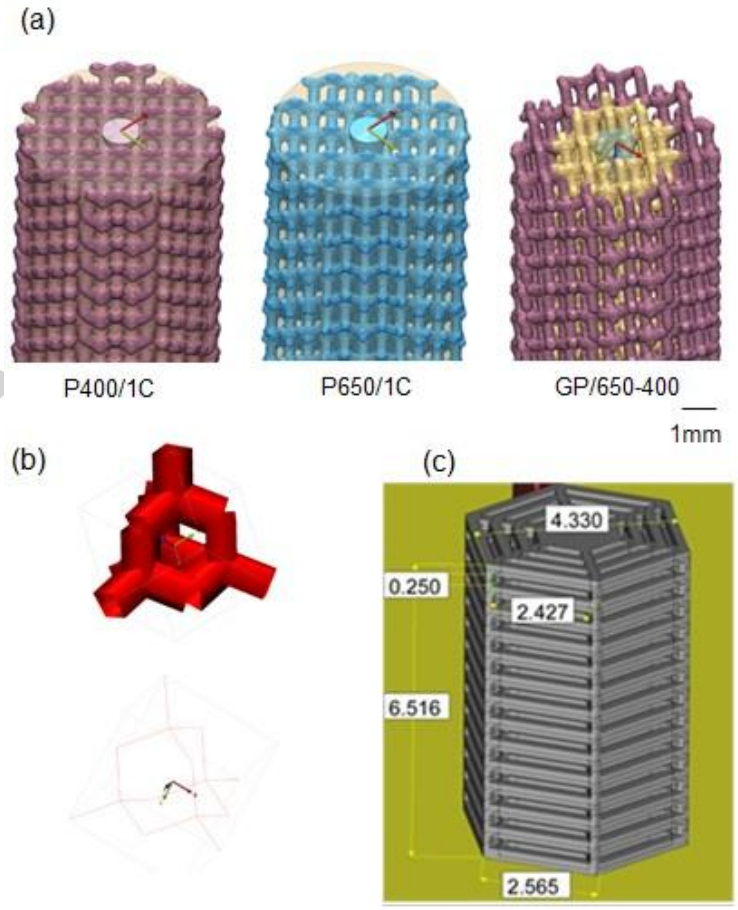

Figure 1. The CAD models of the (a) variant lattices built on the diamond unit cell: P400/1C, P650/1C and GP/650-400, (b) diamond unit cell and (c) 'Spider Web' prototype shown in 3-matics software.

Table 1. A summary of the different lattice designs used here and the nomenclature employed to refer to them in this work. Samples are grouped according to the nominal pore size, strut thickness, and presence or absence of a dense core.

Model type	Pore size (μm)	Strut thickness (μm)	Dense core (mm)
P400	400	400	None
P400/1C	400	400	1
P400/2C	400	400	2
P650	650	300	None
P650/1C	650	300	1
Graded (GP/650-400)	400 (inner layer)	400 (inner layer)	
	650 (outer layer)	300 (outer layer)	1
Graded (GP/400-300)	300 (inner layer)	300 (inner layer)	

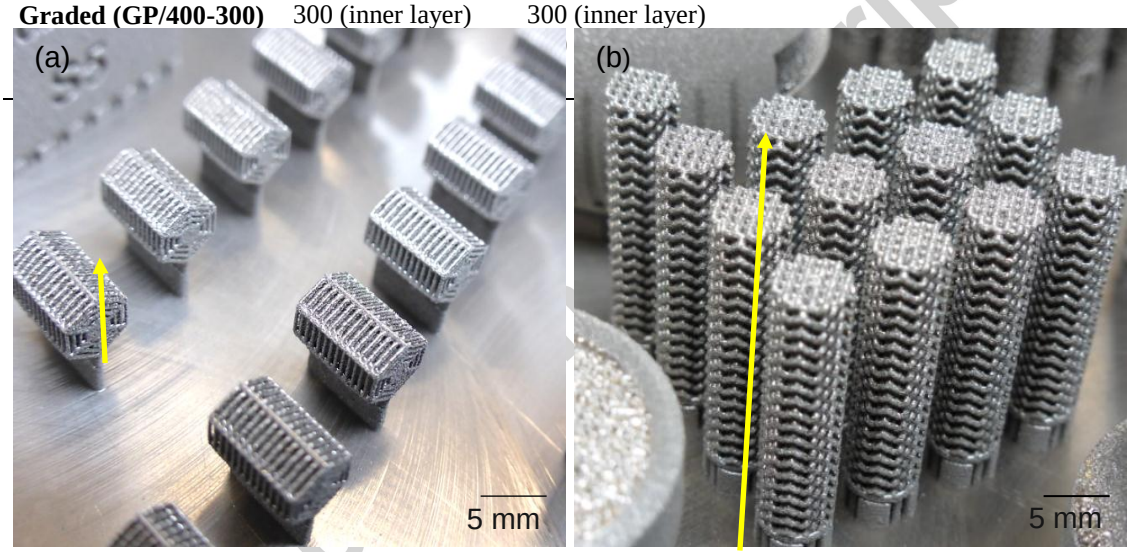

Figure 2. Post-build Ti6Al4V samples of (a) 'Spider Web' (diameter = 4.33 mm and height = 6.76 mm) built horizontally and (b) variant of diamond unit cell lattices built vertically (diameter = 5 mm and height = 20 mm) on the building substrate, yellow arrows indicate building direction.

2.2. Structural Chemistry and Characterization

To evaluate the inner architecture of the pores, titanium components were cut across the axis into cylinders of approximately 7 mm height using a Secotom-50 cutting machine with the cut surfaces ground flat on an Ecomet- 250 grinder-polisher machine, using SiC papers with grits of 500 and then 1000. To remove the loose powders from the built components, they were cleaned for 30 minutes with an ultrasonic bath. These samples were also used to perform both mechanical and biological testing.

Surface chemistry of the built titanium lattices was analysed using Inductively Coupled Plasma Optical Emission Spectroscopy (ICP-OES) to quantify the main elements and LECO (Laboratory Equipment Corporation) to measure the interstitial elements (carbon, oxygen and nitrogen) by AMG Analytical, UK. Pore geometry and interconnectivity were evaluated by SEM (FEI Nova 200, equipped with a field emission gun) and μCT (Skyscan 1172) Bruker system with a medium camera binning mode (2000×1024), 1 mm Al filter and 9.92 μm pixel size. CTAn analysis software was used to analyse the components in three dimensions, 500 cross-sectional images were converted to binary

images with a threshold value of 80, the percentage of the open and total porosity and surface area were calculated. The average pore size and strut thickness were evaluated in Image J software from recorded SEM images. Archimedes method was also used for determining % porosity for fabricated scaffolds according to the equation (1) below and compared with mico-CT results. This method has been used previously in the literature for measuring the density and porosity of porous cylinders [24].

$$\text{Porosity} = (1 - \rho sc / \rho 0) * 100\% \quad (1)$$

where $\rho 0$ is the known density of dense Ti6Al4V (4.43 g/cm^3) and ρsc is the density of the samples, which is measured by the weight of the sample in air (M_a) and water (M_w) using equation (2) below and a Mettler Toledo density balance with 0.1 mg resolution. The density of water ρ_w was assumed to be 1.0 g/cm^3 at room temperature (15-25 °C). To minimise air bubbles distilled water was used at room temperature. [24].

$$\rho sc = ((M_a) / (M_a - M_w)) * \rho_w \quad (2)$$

2.3. Compression testing

The mechanical properties of built Ti-6Al-4V scaffolds around 5 mm diameter and 7 mm height were evaluated in compression according to the international standards ISO 17340:2014 (Metallic materials - Ductility testing - High speed compression test for porous and cellular metals), using a universal testing machine (Zwick Roell) with 1 mm/min speed, 20 kN load cell and 10 kN maximum force. The long axis of the tested samples was oriented perpendicular to the loading direction and the gradient of the core base lattices was radial to the direction of loading. The resulting load-displacement curves were translated to stress-strain curves, the cross sectional area was calculated by measuring the diameter of the samples and used for the calculations of stress and strain. The initial linear elastic region was used to calculate Young's modulus and yield strength using the 0.2% offset strain. Video extensometer provided with the test machine was used during the compression process. Using the recorded videos, silhouette images of the sample changes during compression were obtained.

2.4. Cell culture

2.4.1. Cell seeding

All chemicals used for cell culture were supplied by Sigma-Aldrich (UK) unless otherwise stated. Samples were autoclaved at 121°C for 30 minutes prior to cell seeding. After cooling to room temperature, they were submerged in a culture medium with 30 minutes incubation at 37 °C and 5% CO_2 humid environment to allow protein attachment onto the surface of the scaffolds. The culture medium used was Minimal Essential Medium-α (α-MEM, Lonza, Castleford, UK). It was supplemented with 10% Foetal Bovine Serum (FBS), 1% L-Glutamine solution (0.2 M), 1% Antibiotic solution containing penicillin (10,000 U/mL) and streptomycin (10 mg/mL), Ascorbic Acid-2-Phosphate (AA, 0.2 mM), and β-glycerophosphate (β-GP, 5 mM). Expansion media was removed and MLO-A5s cells were seeded onto the scaffolds by a dipping method in an untreated 24 well plate, using 2,500 cells in 25µl expansion media with 45 minutes incubation for each side of the scaffold to permit cell attachment; negative controls (immersed in media but without cells) were also used. 2mls of EM were added to each scaffold and incubated overnight. Media was changed every 2-3 days during the experiment period and cell viability after seeding was assessed over six different time points. The passage number of cells used for experiments was between 44 -50.

2.4.2. Cell viability assay

Resazurin reduction (RR) metabolic activity assay was used to estimate cell viability on days 1, 4, 7, 14, 21 and 28 of culture. RR solution was prepared by adding 1 mM Resazurin Sodium Salt to deionized water and diluting this to 10 vol % in culture media. For each assay, media was removed from seeded scaffolds, and 2 ml of RR solution was added to each scaffold. Well plates containing scaffolds were wrapped in aluminium foil due to its light sensitivity and incubated for four hours at 37°C. The non-fluorescent blue color of the media was reduced by the metabolic activity of live cells to a fluorescent pink color. In a 96-well plate, 200 µL of the reduced solution was transferred in

triplicate, which was subsequently read with a spectrofluorometer (FLX800, BIO-TEK Instruments, Inc.) at 540 nm excitation wavelength and 590 nm emission wavelength. Fresh culture media was added after twice washing of samples with PBS, with 20 minutes incubation between washes. After the day 28 assay, scaffolds were fixed with 10% formalin for 30 min and kept in PBS prior to calcium and collagen staining.

2.4.3. Alizarin Red S Stain Assay

To determine extracellular calcium deposition, Alizarin Red S (ARS) staining analysis was performed on day 28 of cell culture. Alizarin Red S (ARS) powder was dissolved in deionized water (dH2O) at 1 w/v % and filtered through a 0.2 µm filter to ensure no undissolved particles remain. The fixed scaffolds were cleaned three times with dH2O to remove any remaining formalin solution. Each Sample was submerged in 2 ml of ARS with orbital shaking for 30 minutes at 100 rpm. Then the ARS was removed and any excess was washed off every 5 minutes with dH2O and gentle orbital shaking until the water remained clear. The scaffolds were destained with 5% of perchloric acid on an orbital shaker for 20 minutes. Triplicate samples of 150 µl of destaining solution from each well were added to a clear 96 well plate and absorption was measured at 405 nm in a plate reader.

2.4.3. Sirius Red Stain Assay

To identify collagen deposition within the scaffolds Sirius Red Stain Assay (SRS) was used. Direct red 80 was dissolved in saturated picric acid (1% w/v) with 0.2 µm filter. After the ARS assay was performed the scaffolds were washed three times with dH_2O to remove any of the ARS destain, 2 ml of SRS was then added to each sample. The well plate was placed on an orbital shaker for 18 hours at 100 rpm. The SRS was removed and any excess was washed off with dH_2O. The scaffolds were de-stained with 2 ml of 0.2 M NaOH: methanol (1:1) on an orbital shaker for 20 minutes at 100rpm. Triplicate samples of 150µl of solution from each well plate was added to a clear 96 well plate and absorption was measured at 405nm. For both ARS and SRS a standard curve was prepared from the same working solution and used to obtain concentrations of stain from the absorbance of the eluate.

2.4.4. Statistical analysis

The obtained data are displayed as means ± standard deviation (SD). Preliminary experiments were performed with (n = 6 / group) for P400, P400/1C, P400/2C, P650, P650/1C, (GP/650-400), (GP/400-300) and ‘Spider Web’ scaffolds used to perform compression tests and (n = 9 / group) for biological tests. Data were analysed by a GraphPad Prism 7 software using one or two-way ANOVA with a Tukey's multiple comparisons post-hoc test. $P < 0.05$ was determined to be a statistically significant difference.

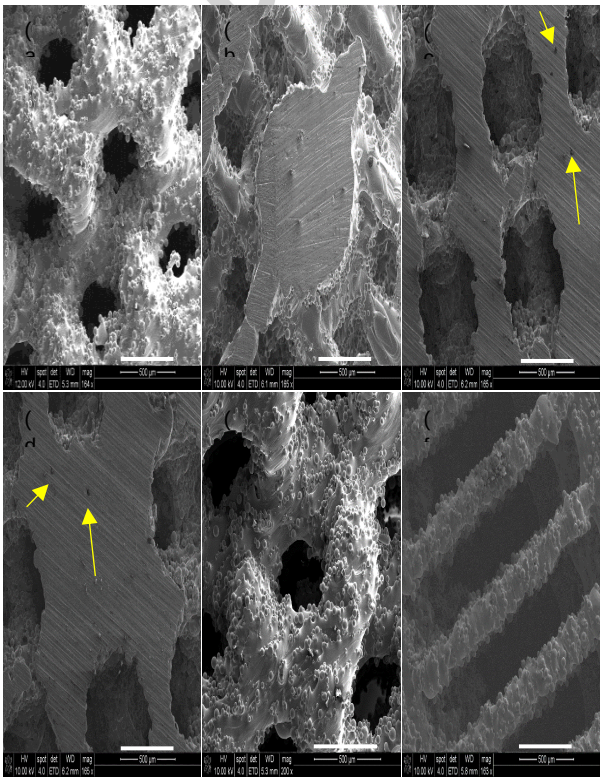

3. Results

3.1. Surface chemistry and structural characterization

The results of the ICP and LECO elemental analysis (supplementary table 1) after production of the SLM Ti-6Al-4V lattices confirmed the Ti, Al and V as the main surface chemistry. The level of O, N and C was about 0.227, 0.044 and 0.023 respectively. These values are close to the content of O (0.13), N (0.08) and C (0.03) as determined in the ASTM B265-08b standard for Grade 23 titanium alloy. The SEM (figure 3) and micro-CT cross-sectional images (figure 4) revealed that selective laser melted constructs of P400, P400/1C, P400/2C, P650, P/C650, GP/650-400, GP/400-300 and spider web had mostly interconnected pores with differing amounts of porosity ranging from 50 to 80%. A very small number of closed micropores (yellow arrows) within the structures were also observed within the lattices (figure 3 c and d). The average open and total porosity are shown in table 2. No statistically significant differences were seen between the open and total porosity, indicating that the porosity present is mostly interconnected. The results for total porosity of titanium lattices, when measured by both the Archimedes method and micro-CT, were similar as shown in (table 2). The struts are well-defined and continuous. The ratio between the object surface area to volume ratio increased with increasing porosity. The average pore size, average strut thickness and the percentages of open, closed and total porosity and object surface to volume ratio of variable titanium lattices P400, P400/1C, P400/2C, P650, P650/1C, GP/650-400, GP/400-300 and spider web are shown in table 2.

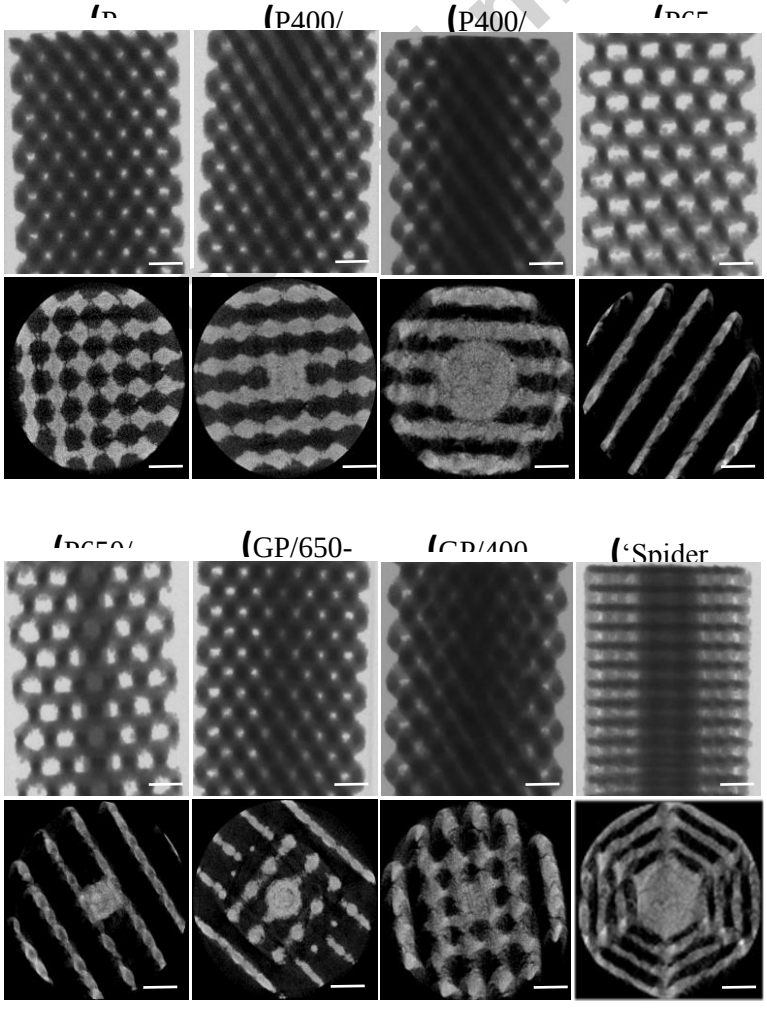

Figure 3. SEM images of diamond unit cell lattices a- P400, b- P400/1C, c- P650, d- P650/1C, e- GP/650-400 and f-'Spider Web', yellow arrows indicate closed porosity, (scale bar: 500 μm).

Figure 4. MicroCT reconstruction images, top (lateral view) and bottom (cross - section) of P400, P400/1C, P400/2C, P650, P650/1C, GP/650-400, GP/400-300 and 'Spider Web' lattices, (scale bar: 1mm).

Table 2. Mean ± S.D of average pore size, average strut thickness and the percentages of open, closed and total porosity and object surface to volume ratio of variable titanium lattices calculated by 3 D analysis of the micro-CT cross-sectional images using CTAn software. Total porosity was also measured by the Archimedes method. These data were performed on 3 samples for each group, the average pore size and strut thickness were analyzed using Image J (n=300).

Groups	Average pore size μm	Average strut thickness μm	Object surface / volume ratio	Open porosity %	Closed porosity %	Total porosity %	Porosity% By Archimedes
P400	411 ± 13	421 ± 28	16.6 ± 0.6	56.8 ± 1.0	0.29 ± 0.10	56.9 ± 1.0	55.2 ± 3.0
P400/1C	421 ± 15	412 ± 22	12.3 ± 0.6	51.2 ± 0.4	0.04 ± 0.03	51.5 ± 0.4	51.8 ± 4.5
P400/2C	423 ± 24	422 ± 11	17.0 ± 1.6	48.4 ± 0.9	0.30 ± 0.02	48.6 ± 1.1	47.6 ± 2.4
P650	654 ± 25	314 ± 21	22.1 ± 0.8	82.8 ± 0.8	0.08 ± 0.02	82.9 ± 0.7	80.4 ± 3.6
P/C650	645 ± 13	333 ± 22	20.6 ± 1.6	80.9 ± 0.6	0.05 ± 0.01	80.9 ± 0.6	79.0 ± 2.9
GP/650-400	655 ± 25 /420 ± 16	302 ± 19 /433 ± 20	19.2 ± 1.1	78.5 ± 0.4	0.12 ± 0.04	78.5 ± 0.4	76.1 ± 2.2
GP/400-300	420 ± 25 /305 ± 123	414 ± 23 /315 ± 27	17.9 ± 0.3	56.6 ± 0.8	0.18 ± 0.04	56.7±0.8	55.7 ± 1.7
Spider Web	254 ± 12	230 ± 18	20.2 ± 1.8	68.5 ± 1.6	0.320 ± 0.1	68.6±1.5	67.4 ± 1.4

3.2. Mechanical testing

Stress-strain values of titanium lattices under compression (supplementary figure 1) showed an overall linear relationship in the elastic region and then plastic yield plateau. Six linear elastic regions of each design showed a highly reproducible pattern. The failure mode for the titanium lattices of P400, P400/1C, P650, P650/1C, GP/650-400, and 'Spider Web' (supplementary figure 2) showed that the deformation of the core-base lattices structure exposing initial core buckling and then lattices break before structure collapse. While structures without a dense core exposed a plastic lattices breakdown starting from the top and bottom sides of samples leading to structure rupture.The Young's modulus and yield strength of the regular and graded scaffolds were similar between samples of the same design, with a low standard deviation, indicating the scaffold manufacture had high reproducibility with respect to bulk mechanical properties (table 3). There were higher mechanical properties in samples with a dense core and thicker struts. The highest Young's moduli and yield strengths were exhibited by scaffolds with a 'spider web' structure and 2 mm dense core, while the

weakest scaffolds were with P650. When comparing the same lattice pore sizes where both structures have a core, e.g. 400/1C compared with GP/400-300 (supplementary table 2) there were no significant differences between graded structures and non graded structures in compression modulus or strength. With increasing porosity, Young's modulus and yield strength were lower, as would be expected (figure 5). Most samples lie on the same general curve on a plot of mechanical properties against density, but the spider web design is notably higher for a given density. This probably reflects the lower degree of isotropy in this structure, being particularly mechanically efficient along the axial direction tested.

Table 3. Mechanical properties (Young's modulus and yield strength) of all Ti6Al4V lattices (Mean ± SD).

Groups	**Young's Modulus (GPa)**	**Yield Strength (MPa)**
P400	3.3 ± 0.6	147 ± 10
P400/1C	4.1 ± 0.3	178 ± 10
P400/2C	4.8 ± 0.6	204 ± 33
P650	0.7 ± 0.2	16 ± 4
P650/1C	2.0 ± 0.3	55 ± 4
GP/650-400	1.7 ± 0.2	48 ± 1
GP/400-300	3.4 ± 0.4	147± 31
'Spider Web'	6.0 ± 0.4	224 ± 7

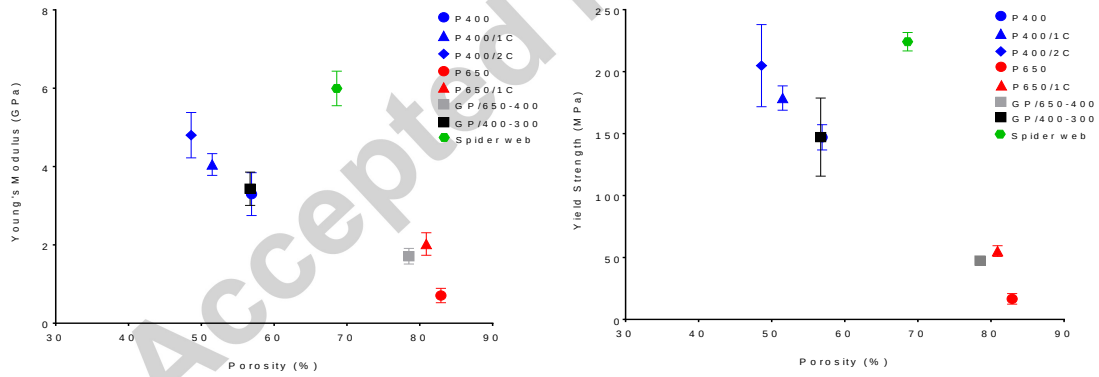

Figure 5. A comparison of the mechanical properties (a) Mean ± SD Young's modulus, (b) Mean ± SD yield strength of the regular and graded Ti5Al4V lattices plotted against % mean porosity by volume as assessed by CT scan.

3.2. Cell Culture

3.2.1. Cell viability on titanium scaffolds

Cell culture assays on P400, P400/1C, P650, P650/1C, GP/650-400 and 'Spider Web' indicated that cells were evidently viable in all the porous structures over 28 days. Generally, the attachment of bone cells across scaffolds was comparable; the viability increased steadily from day 4 to day 7 in all scaffolds without significant differences at each time point. Interestingly, the results indicate that large pore sizes (650 microns) do not enhance cell ingrowth and confirm that any pore size between 250 and 650 microns is a supportive structure for bone cells. Similar metabolic activity of bone cells was obtained from the P400, P400/1C, P400/2C, GP400-300 and 'Spider Web' scaffolds (figure 6 (a)).

3.2.2. Calcium and collagen staining

Calcified matrix staining on day 28 of cell culture indicated that all structures supported mineral production. Alizarin red absorbance for cells seeded on P400 scaffolds was significantly higher than that on 'Spider Web' scaffolds, (figure 6 (b)). A similar result was observed for collagen analysis, where all scaffolds support extracellular matrix production. However, there were no significant differences across the seeding groups (figure 6 (c)).

(a)

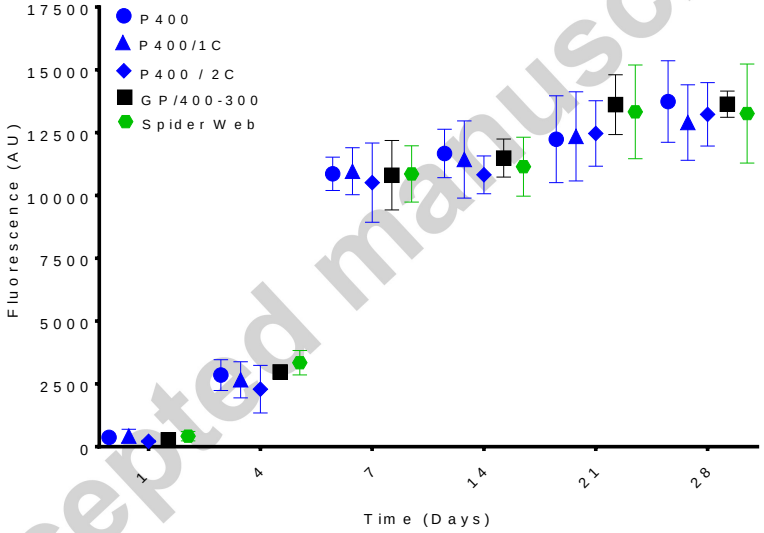

(b)

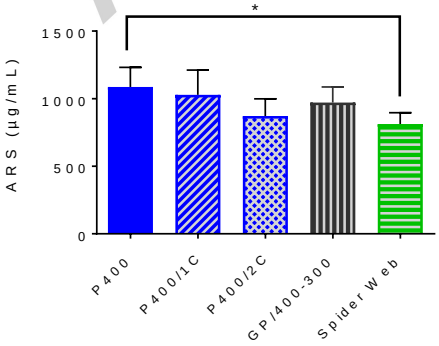

(c)

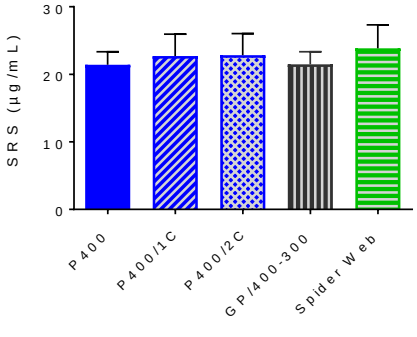

Figure 6. Mean ± SD for (a) resazurin fluorescence as a measure of cell viability of MLO-A5s on P400, P400/1C, P400/2C, GP/400-300 and 'Spider Web' scaffolds over 28 days (b) ARS staining and (c) SRS staining on day 28 of cell culture, (n=9).

4.2. Discussion

In an effort to evaluate the feasibility of SLM to produce complex geometries of titanium for their use in dental implants to improve bone ingrowth and implant stability, a range of porous titanium scaffolds with variable porosity were developed based on an approximate cylindrical shape of a size representing that of a dental implant. Structures were created with uniform and graded porosity using different pore shape, size and percentage with and without a dense core, designated as P400, P400/1C, P400/2C, P650, P650/1C, GP/650-400, GP/400-300 and 'Spider Web'. The structural and mechanical properties of the resulting structures were evaluated, and assessed biologically by seeding with bone cells for up to 28 days.

Several previous studies have evaluated the impact of porosity and pore shape of porous structures on the biological response to bone cells. Most of these studies focused on creating porous coatings on implants with pore sizes below 200 μm. Creating a uniform and large pore size has been recommended to achieve good bone ingrowth and vascularization. In this study, we aimed to examine highly regular lattice structures with specific pore sizes (250, 300, 400 and 650 μm) in terms of their biofunctional performance. SLM was chosen to produce titanium lattices due to its potential to be used for the production of controllable and homogeneous pore sizes. Titanium alloy Ti6Al4V is widely used for SLM to produce medical devices. Although titanium and its alloys have been reported to be bioinert and biocompatible materials for dental and orthopaedic implants [25], it is necessary that constructs from these materials produced via advanced manufacturing technology are evaluated for biofunctional properties.

The unit cell of choice used was a diamond lattice (figure 1 (b)), because it is a simple structure which has a relatively low stiffness relative to its density and has been previously used for similar medical applications to mimic the properties of cancellous bone [22]. A novel design of 'Spider Web' was also used and compared as this was an effective way to produce a graded pore structure but to our knowledge such a radial pore structure has never been assessed for its suitability for a medical implant design.

The low interstitial elements value in the built SLM Ti-6Al-4V structures when compared to the higher levels found with titanium foams produced by different fabrication methods such as metal injection moulded [15] indicates the low risk of contamination with SLM process which may excepect less effect on the strength properties. The degree of porosity in the built lattices was controlled via changing the pore size and strut thickness. The different approaches for determining porosity revealed a high level of agreement. The results for the total porosity, when measured by the Archimedes and micro-CT methods, were generally comparable (table 2), though there was higher variability for the lattices porosities measured by Archimedes. Although an attempt was made to minimise the presence of air bubbles these could still have been present, leading to a higher measured density to be measured and lower apparent porosity. This finding is in agreement with the study of Slotwinski *et al.*, which showed general agreement in porosity measurement of additively manufactured CoCr components using Archimedes, mass/volume, and X-ray CT [24].

The stress-strain curves of the different Ti-6Al-4V lattices used in this study are relatively typical of what we see for these kinds of lattice materials [22]. One factor is that they are more highly reproducible sample-to-sample than random structured porous materials, such as foams and sponges. This is due to the structure of each sample being more highly repeatable. For the actual stress-strain curves, there is an initial elastic stage (approximately linear) corresponding to bending of the struts but giving rise to a lower gradient than a dense material would. Then there is a yield event where a particular strut fails, which may be followed by some degree of work hardening, like in a solid, but which more commonly leads to a decrease in load as part of the structure collapses into the available free space, in the manner of a porous solid. In terms of the mechanism (supplementary figure 2), at a

mesoscale we identify that collapse begins in one horizontal layer, on a random basis, likely mediated by a defect. This layer then proceeds to crush to a high density, before the stress raises in another layer to a sufficiently high level to initiate failure and the process repeats. This is the origin of the cycles seen most clearly in the P400 sample (though present in some others); each peak is the point of failure initiation in a new layer, which causes a drop in load. Once the layer is crushed, the load starts to build up again. The uniform size of the layers explains the uniform engineering strain level over which the repeats occur. This progressive failure is significantly affected in a solid core, as this resists collapse and causes more distributed deformation. In such samples we do not see the repeated cycles of load increase and decrease. While the samples here were not examined at sufficient detail to draw conclusions on the mechanism of failure in individual struts, from other work on EBM lattices it is known that the struts generally display very limited plasticity [26], and so the failure is likely to be in a brittle mode.

As would be expected, the differences in porosity result in differences in Young's modulus and yield strength, which are lower at higher porosities. A large variety of values have been reported for Young's modulus of cancellous bone depending on species, preparation methods and types of bone, for example, the range for cancellous bone in the mandible is 1.5-4.5 GPa as reviewed in the literature [27]. A lower range of Young's modulus (0.1 - 2 GPa) also been reported [28]. The structures used in this study were of a similar range to these values ranging from 0.7 - 6 GPa. The root part of the natural tooth is made from dentine which is covered by cementum, tooth is held into the bone via periodontal ligament. Forces of mastication for each tooth are transferred from enamel through dentine to the root, then from cementum through the periodontal ligament to the cancellous bone to the end at the ramus of the jaw [29]. In the literature there is some debate about the Young's modulus of dentine, generally it is reported as around 20-25 GPa [30] which is comparable to cortical bone (17–20 GPa) [2]. However, in artificial implants there is a direct contact between bone and the implant structure which induces bone ingrowth. Dental implants should withstand the physiological function during mastication. The maximum biting force is from 230 - 450 N in the molar region [28].

Compression testing was performed in this study to compare the basic structural mechanical properties of structures which were produced from different batches, all scaffolds demonstrated a highly reproducible behavior, which is attributed to the uniform geometry of the SLM lattices. This is in agreement with previous work in our laboratory on cubes of lattice structures in which a highly reproducible initial elastic region of the stress-strain curve was exhibited by Ti6Al4V scaffolds built on diamond unit cell and produced via EBM [31]. Strength properties of porous biomaterials can be improved with increasing density [32]. Interestingly, 'Spider Web' lattices were the strongest scaffolds in compression in relation to their porosity. A possible explanation for this result may be the lower degree of isotropy in this structure, being particularly mechanically efficient along the axial direction tested. Recent research has shown that additively manufactured structures exhibit anisotropic behaviour [33], but that this difference becomes insignificant for larger unit cells, and derives from the smaller samples in that work not accurately replicating the CAD model shape - the anisotropy in property comes from differences in the porous structure, not inherent directionality in the properties of the metal from which it is made.

The only structures which did not have adequate strength compared to bone were the non-core based lattices with a 650 µm pore size and 300 µm strut thickness (P650) which were the least stiff and strong scaffolds. This is likely because these were the highest porosity structures and so had the least amount of solid to resist deformation. Previous research has also documented that completely porous metal structures for both orthopaedics or dental implants are not able to provide sufficient strength to withstand physiological loading [20]. To improve the mechanical properties, a compact dense core was incorporated into the structures. As expected, core based lattices were stronger than the entirely porous scaffolds. This finding has also been confirmed in the literature, where implants with two different zones, a dense core and irregular porous shell have been found to be more appropriate for load bearing devices such as dental implants, such as in a study with a dental root implant produced by incorporating selective laser sintering for the porous coating and selective laser melting for the dense core [17]. A major advantage of SLM is that the porous structure and a solid core are made in

one build of one material, compared to making a structure first and then combining this with a porous coating. Structural modifications including increasing the diameter of the dense core of the regular pore structures and strut thickness of the graded structures result in significant improvement of Young's modulus and yield strength (Table 2), as there is then more solid to support load.

Implants with graded porosity enable rapid bone ingrowth while the low-porosity part of the component provides strength to sustain the physiological load [34]. The deformation mechanisms of uniform and graded porous structures for stretching and bending were studied by Afshar *et al*. They concluded that graded structures deform less than uniform ones. They also stated that the energy absorption and elastic–plastic deformation were high for struts oriented in the loading direction [35]. In terms of mechanical properties found in our tests, the graded structures have properties that roughly correspond with their overall density. This is to be expected as they have been tested with the different density regions (and dense core if present) in parallel, and shows that the properties combine arithmetically, rather than there being more complex interactions between the different density layers. This is in agreement with earlier work [22] where the layers were tested in series, and elastic deformation was found to spread according to Young's modulus, and plastic deformation to progress from the lowest density layer to the highest. Were the samples here to be tested in bending, where the outer layers experience higher strain than the centre, the difference between the graded and non-graded lattices would be more significant. These results demonstrate the feasibility to design overall mechanical properties by combining different lattices in a graded structure.

In *in vitro* cell culture on P400, P400/1C, P400/2C, GP400-300 and 'Spider Web' designs showed that osteoblastic cells readily attached to porous Ti6Al4V. Implants with rough surfaces have been shown to promote osteoblast cells attachment [36], and proliferation as referred by Karageorgiou and Kaplan [37]. The metabolic activity of cells showed significant increases over 28 days of cell culture (figure 6), likely due to a large surface area which promotes cell proliferation, and subsequent extracellular matrix production. Previous research has indicated that porous titanium surfaces have a positive effect on bone cell growth and matrix production. Stevenson *et al.* examined the potential of osteosarcoma cell line (MG63) and primary human osteoblast cells to proliferate and mineralize on titanium surfaces with different porosities [24]. In that study fine surface coatings supported less mineralization than coarse surfaces. Interconnected porosity has also been shown to induce the attachment and proliferation of bone cells [34] such as a graded porous structure of different materials HA-$CaCO_3$-Ti with macro- (100-350 μm), micro- (0.2–90 μm) and nano-(100 nm) porosity which stimulated bone formation [38]. Our study shows no significant variation in cell viability when comparing scaffolds with different pore size, shape and percentage. This result is in agreement with Cheng et al., where even with the high metabolic activity of osteoblasts (MG63 cells) that has been observed on porous titanium constructs with average pore diameter 177, 383 and 653, there were no differences shown among variant scaffolds [39]. Nevertheless, Markhoff *et al*. evaluated the metabolic activity of human osteoblast cells on porous titanium scaffolds with cubic, pyramidal and diagonal basic structures under static and dynamic culture. They reported a significantly higher metabolic cell activity on pyramidal basic structure scaffolds with 400-620 μm pore size and 75% porosity with no significant differences between the culture methods [40]. In another *in vitro* observation, human osteoblasts cells were cultured on direct laser formed Ti-6Al-4V porous scaffolds with 500, 700 and 1000 μm pore size, after 14 days of cell culture cells covered most of the pores with 500 μm pore size. While the pore size of 700 and 1000 μm formed a circular-shaped growth pattern around the pore walls [41].

Overall, all scaffolds supported calcium and collagen formation indicating their suitability to support bone ingrowth; scaffolds with P400 exhibited the highest calcium deposition. Pore sizes between 100 and 400 μm are suggested for bone mineralization [20]. Our study showed no effect of pore size and shape on matrix production by MLOA5s. As can be observed the effect of pore size on matrix growth is not straightforward and is probably governed by contributing factors such as roughness or pore wall size or structure and nutrient accessibility. Frosch *et al.* have also demonstrated that collagen production is not influenced by the pore size (over the range 300-1000 μm) of titanium scaffolds [42]. In contrast to our study indicating no effect of pore shape; within the structures used by Markhoff *et*

al. collagen formation was significantly less supported on diagonal compared to cubic and pyramidal structures [40]. Based on our results, all Ti6Al4V scaffolds were shown to sustain MLOA5s cell viability and mineralization. However, MLOA5s are prone to proliferate rapidly and produce a lot of matrix, and more subtle differences may be seen with primary human cells. Further *in vitro* experiments can be performed to investigate the behaviour of these scaffolds with primary cells.

5. Conclusion

In conclusion, here we verified that the SLM technique could produce a range of well-controlled porous Ti6Al4V structures with uniform and graded porosity of a suitable size for dental implants. All structures had compressive mechanical properties in the range of those previously reported for cancellous bone, except for the 650-micron pore size scaffolds. The presence of a dense core led to an improvement in the compressive mechanical properties of the lattice structures while graded structures were found to behave in line with their average density. All structures strongly supported cell growth and mineralized matrix deposition which was not affected by pore size except that the maximum calcium deposition was seen on scaffolds with 400-micron pores. Although it did not support maximal calcium deposition, the spider web scaffold seems to strike a balance between good resistance to compression and high porosity and may be a promising structure to take forward to incorporate into a dental implant-shaped structure. Overall this technique is extremely promising as a fabrication method for dental implants which could be more cost-effective and allow better osseointegration than those currently available.

Acknowledgements

Authors would like to thank The Medical Advanced Manufacturing Research Centre (AMRC) for access to equipment to manufacture the experimental scaffolds and Iraqi Ministry of Higher Education and Scientific Research for funding.

6. References

[1] Mehrali M, Shirazi F S, Mehrali M, Metselaar H S C, Kadri N A B and Osman N A A 2013 Dental implants from functionally graded materials. *J. Biomed. Mater. Res. A* **101** 3046–57

[2] Wally Z, van Grunsven W, Claeyssens F, Goodall R and Reilly G 2015 Porous Titanium for Dental Implant Applications *Metals (Basel).* **5** 1902–20

[3] Elias C N 2011 *Factors Affecting the Success of Dental Implants,* ed I dentistry-a rapidly evolving practice Turkyilmaz I (New York: InTech) P 319-364

[4] Deporter D, Pharoah M, Yeh S, Todescan R and Atenafu E G 2014 Performance of titanium alloy sintered porous-surfaced (SPS) implants supporting mandibular overdentures during a 20-year prospective study. *Clin. Oral Implants Res.* **25** e189-95

[5] Mangano F G, Caprioglio A, Levrini L, Farronato D, Zecca P A and Mangano C 2015 Immediate Loading of Mandibular Overdentures Supported by One-Piece, Direct Metal Laser Sintering Mini-Implants: A Short-Term Prospective Clinical Study. *J. Periodontol.* **86** 192–200

[6] Gaviria L, Salcido J P, Guda T and Ong J L 2014 Current trends in dental implants. *J. Korean Assoc. Oral Maxillofac. Surg.* **40** 50–60

[7] Mendonça G, Mendonça D B S, Aragão F J L and Cooper L F 2008 Advancing dental implant surface technology--from micron- to nanotopography. *Biomaterials* **29** 3822–35

[8] Junker R, Dimakis A, Thoneick M and Jansen J A 2009 Effects of implant surface coatings and composition on bone integration: a systematic review. *Clin. Oral Implants Res.* **20 Suppl 4** 185–206

[9] Nouri A, Hodgson P D and Wen C 2010 Biomimetic Porous Titanium Scaffolds for Orthopedic and Dental Applications, in Mukherjee A (eds.) Biomimetics Learning from Nature, InTech Pub, pp. 415–50

[10] Wu S, Liu X, Yeung K W K, Liu C and Yang X 2014 Biomimetic porous scaffolds for bone tissue engineering *Mater. Sci. Eng. R Reports* **80** 1–36

[11] Oh S H, Park I K, Kim J M and Lee J H 2007 In vitro and in vivo characteristics of PCL scaffolds with pore size gradient fabricated by a centrifugation method. *Biomaterials* **28** 1664–71

[12] Vasconcellos L M R, Leite D O, Nascimento F O, Vasconcellos L G O, Graça M L A, Carvalho Y R and Cairo C A A 2010 Porous titanium for biomedical applications: an experimental study on rabbits. *Med. Oral Patol. Oral Cir. Bucal* **15** 407-12

[13] Fernández M P R, Gehrke S A, Mazón P, Calvo-Guirado J L and De Aza P N 2017 Implant stability of biological hydroxyapatites used in dentistry *Materials.* **10** 1-15

[14] Vasconcellos L M R De, Oliveira M V D, Graça M L D A, Vasconcellos L G O D, Carvalho Y R and Cairo C A A 2008 Porous titanium scaffolds produced by powder metallurgy for biomedical applications *Mater. Res.* **11** 275–80

[15] Shbeh M M and Goodall R 2015 Design of water debinding and dissolution stages of metal injection moulded porous Ti foam production *Mater. Des.* **87** 295–302

[16] Koike M, Greer P, Owen K, Lilly G, Murr L E, Gaytan S M, Martinez E and Okabe T 2011 Evaluation of Titanium Alloys Fabricated Using Rapid Prototyping Technologies—Electron Beam Melting and Laser Beam Melting *Materials (Basel).* **4** 1776–92

[17] Tolochko N K, Savich V V., Laoui T, Froyen L, Onofrio G, Signorelli E and Titov V I 2002 Dental root implants produced by the combined selective laser sintering/melting of titanium powders *Proc. Inst. Mech. Eng. Part L J. Mater. Des. Appl.* **216** 267–70

[18] Mullen L, Stamp R C, Brooks W K, Jones E and Sutcliffe C J 2009 Selective Laser Melting: a regular unit cell approach for the manufacture of porous, titanium, bone in-growth constructs, suitable for orthopedic applications. *J. Biomed. Mater. Res. B. Appl. Biomater.* **89** 325–34

[19] Moin D A, Hassan B, Mercelis P and Wismeijer D 2013 Designing a novel dental root analogue implant using cone beam computed tomography and CAD/CAM technology. *Clin. Oral Implants Res.* **24** 25–7

[20] Ryan G, Pandit A and Apatsidis D P 2006 Fabrication methods of porous metals for use in orthopaedic applications. *Biomaterials* **27** 2651–70

[21] Laoui T, Santos E, Osakada K, Shiomi M, Morita M, Shaik S K, Tolochko N K, Abe F and Takahashi M 2006 Properties of Titanium Dental Implant Models Made by Laser Processing *Proc. Inst. Mech. Eng. Part C J. Mech. Eng. Sci.* **220** 857–63

[22] van Grunsven W, Hernandez-Nava E, Reilly G and Goodall R 2014 Fabrication and Mechanical Characterisation of Titanium Lattices with Graded Porosity *Metals (Basel).* **4** 401–9

[23] Joshi G V, Duan Y, Neidigh J, Koike M, Chahine G, Kovacevic R, Okabe T and Griggs J A 2013 Fatigue testing of electron beam-melted Ti-6Al-4V ELI alloy for dental implants. *J. Biomed. Mater. Res. B. Appl. Biomater.* **101** 124–30

[24] Slotwinski J A, Garboczi E J and Hebenstreit K M 2014 Porosity Measurements and Analysis for Metal Additive Manufacturing Process Control. *J. Res. Natl. Inst. Stand. Technol.* **119** 494–528

[25] Stevenson G, Rehman S, Draper E, Hernandez-Nava E, Hunt J and Haycock J W 2016 Combining 3D human in vitro methods for a 3Rs evaluation of novel titanium surfaces in orthopaedic applications *Biotechnol. Bioeng.* **113** 1586–99

[26] Hernandez-Nava E, Smith C J, Derguti F, Tammas-Williams S, Leonard F, Withers P J, Todd I, Goodall R 2016 The effect of defects on the mechanical response of Ti-6Al-4V cubic lattice structures fabricated by electron beam melting. *Acta Mater.* **108** 279–292

[27] Andani M T, Moghaddam N S, Haberland C, Dean D, Miller M J and Elahinia M 2014 Metals for bone implants. Part 1. Powder metallurgy and implant rendering. *Acta Biomater.* **10** 4058–70

[28] Wen C (ed.) 2017 Metallic foam bone, Woodhead Pub./Elsevier, Oxford

[29] Currey J D 2012 The structure and mechanics of bone J. Mater. Sci. 47 41–54

[30] Kinney J H, Marshall S J and Marshall G W 2003 The mechanical properties of human dentin: a critical review and re-evaluation of the dental literature. Crit. Rev. Oral Biol. Med. 14 13–29

[31] Van Grunsven W 2014 *Porous metal implants for enhanced bone ingrowth and stability Ph.D. Thesis*, University of Sheffield, Sheffield, UK, September 2014.

[32] Balla V K, Bodhak S, Bose S and Bandyopadhyay A 2010 Porous tantalum structures for bone implants: fabrication, mechanical and in vitro biological properties. *Acta Biomater.* **6** 3349–59

[33] Ataee A, Li Y, Fraser D, Song G and Wen C 2018 Anisotropic Ti-6Al-4V gyroid scaffolds manufactured by electron beam melting (EBM) for bone implant applications *Mater. Des.* **137** 345–54

[34] Soon Y-M, Shin K-H, Koh Y H, Lee J-H, Choi W-Y and Kim H-E 2011 Fabrication and compressive strength of porous hydroxyapatite scaffolds with a functionally graded core/shell structure *J. Eur. Ceram. Soc.* **31** 13–8

[35] Afshar M, Anaraki A P, Montazerian H and Kadkhodapour J 2016 Additive manufacturing and mechanical characterization of graded porosity scaffolds designed based on triply periodic minimal surface architectures J. Mech. Behav. Biomed. Mater. 62 481–94

[36] Mour M, Das D, Winkler T, Hoenig E, Mielke G, Morlock M M and Schilling A F 2010 Advances in Porous Biomaterials for Dental and Orthopaedic Applications *Materials (Basel).* **3** 2947–74

[37] Karageorgiou V and Kaplan D 2005 Porosity of 3D biomaterial scaffolds and osteogenesis. *Biomaterials* **26** 5474–91

[38] Fu Q, Hong Y, Liu X, Fan H and Zhang X 2011 A hierarchically graded bioactive scaffold bonded to titanium substrates for attachment to bone. *Biomaterials* **32** 7333–46

[39] Cheng A, Humayun A, Cohen D J, Boyan B D and Schwartz Z 2014 Additively manufactured 3D porous Ti-6Al-4V constructs mimic trabecular bone structure and regulate osteoblast proliferation, differentiation and local factor production in a porosity and surface roughness dependent manner. *Biofabrication* **6** 045007

[40] Markhoff J, Wieding J, Weissmann V, Pasold J, Heincke A J and Bader R 2015 Influence of Different Three-Dimensional Open Porous Titanium Scaffold Designs on Human Osteoblasts Behavior in Static and Dynamic Cell Investigations *Materials (Basel).* **8** 5490–507

[41] Hollander D A, Von Walter M, Wirtz T, Sellei R, Schmidt-Rohlfing B, Paar O and Erli H-J 2006 Structural, mechanical and in vitro characterization of individually structured Ti-6Al-4V produced by direct laser forming. *Biomaterials* **27** 955–63

[42] Frosch K-H, Barvencik F, Viereck V, Lohmann C H, Dresing K, Breme J, Brunner E and Stürmer K M 2004 Growth behavior, matrix production, and gene expression of human osteoblasts in defined cylindrical titanium channels. *J. Biomed. Mater. Res. A* **68** 325–34

Highlights:

- In a one-step process, small rod-like parts, with graded porosity, of an appropriate size for dental implants can be prepared by selective laser melting.
- Ti6Al4V lattices with graded and regular porosity form suitable stuctures for bone cell ingrowth, with mechanical properties comparable to cancellous bone.
- Structures with a solid core, radial porosity and a spider-web appearance in cross section have high compressive strength relative to their high porosity.
- Ti6Al4V lattices may improve bone integration and stability of dental implants in elderly and diabetic people with poor bone healing.